Journal of Inorganic Biochemistry 193 (2019) 152–165

Contents lists available at ScienceDirect

Journal of Inorganic Biochemistry

journal homepage: www.elsevier.com/locate/jinorgbio

A new tripodal kojic acid derivative for iron sequestration: Synthesis, protonation, complex formation studies with Fe^{3+}, Al^{3+}, Cu^{2+} and Zn^{2+}, and *in vivo* bioassays

Valeria M. Nurchi[a], Maria de Guadalupe Jaraquemada-Pelaez[b], Guido Crisponi[a,*], Joanna I. Lachowicz[a], Rosita Cappai[a], Lurdes Gano[c], M. Amelia Santos[d], Andrea Melchior[e], Marilena Tolazzi[e], Massimiliano Peana[f], Serenella Medici[f], Maria Antonietta Zoroddu[f]

[a] Department of Life and Environmental Sciences, University of Cagliari, Cittadella Universitaria, Monserrato, Cagliari, Italy
[b] Medicinal Inorganic Chemistry Group, Department of Chemistry, University of British Columbia, Vancouver, BC, Canada
[c] Centro de Ciências e Tecnologias Nucleares (C2TN), Instituto Superior Técnico, Universidade de Lisboa, Estrada Nacional 10, 2695-066 Bobadela LRS, Portugal
[d] Centro de Química Estrutural, Instituto Superior Técnico, Universidade de Lisboa, Av. Rovisco Pais 1, 1049-001 Lisboa, Portugal
[e] Dipartimento Politecnico, Laboratori di Tecnologie Chimiche, Università di Udine, Via del Cotonificio 108, 33100 Udine, Italy
[f] Dipartimento di Chimica e Farmacia, Università di Sassari, Sassari, Italy

ARTICLE INFO

Keywords:
Hydroxypyrones
Tris-hydroxypyrone chelator
Kojic acid
Metal complexation
Solution studies
In vivo bioassays

ABSTRACT

This work presents the simple and low cost synthesis of a new tripodal ligand, in which three units of kojic acid are coupled to a tris(2-aminoethyl)amine (tren) backbone molecule. The protonation equilibria, together with the complex formation equilibria of this ligand with Fe^{3+}, Al^{3+}, Cu^{2+} and Zn^{2+} ions were studied. The complementary use of potentiometric, spectrophotometric and NMR techniques, and of Density Functional Theory (DFT) calculations, has allowed a thorough characterization of the different species involved in equilibrium. The stability of the formed complexes with Fe^{3+} and Al^{3+} are high enough to consider the new ligand for further studies for its clinical applications as a chelating agent. Biodistribution studies were carried out to assess the capacity the ligand for mobilization of gallium in ^{67}Ga-citrate injected mice. These studies demonstrated that this ligand efficiently chelates the radiometal in our animal model, which suggests that it can be a promising candidate as sequestering agent of iron and other hard trivalent metal ions. Furthermore, the good zinc complexation capacity appears as a stimulating result taking into a potential use of this new ligand in analytical chemistry as well as in agricultural and environmental applications.

1. Introduction

The present study is part of a research project on iron chelating agents for clinical use that we are carrying out along the last ten years [1]. Furthermore, according to the chemical and physical features of the chelators, these can also find application in a variety of fields, as environmental chemistry [2–4], agriculture [5,6] and analytical chemistry. The research we developed in the last years has been centered on tetradentate derivatives of kojic acid (KA) (Fig. 1), obtained by connecting two KA units through linkers anchored in position 6 [7–9], with variations in chemical nature, length, charge, *etc*. These linkers can provide molecules not only with different chelating properties, but also with different chemical and physical features that determine the properties of the molecule *in vivo* (as intestinal absorption, cellular permeability, bioavailability, and pharmacokinetics). Assembling two KA units in a unique ligand leads to an increase of the stability of the formed iron complexes: the pFe[1] passes from 13.1 for KA to values up to 18–20 for the bis-derivatives. The enthalpic contribution to the stability of the iron complexes with tetradentate ligands should be similar to that of KA, thus, not disturbed by strain effects. Consequently, it is the entropic contribution, due to the preorganization of KA moieties, which determines the remarkable increase of the iron chelating capacity and associated pFe value. Recently, we used a different synthetic strategy, based on connecting two KA units through linear diamines of different

* Corresponding author at: University of Cagliari, Cittadella Universitaria, 09042 Monserrato, Cagliari, Italy.
E-mail address: crisponi@unica.it (G. Crisponi).

[1] pFe is the parameter generally used for evaluating the chelating ability of a ligand, independent both on the proton competition with iron for the same coordinating sites and on the stoichiometry of the formed complexes. It is defined as the concentration, expressed as negative logarithm, of free Fe^{3+} in a solution at pH 7.4 that is 1 μM in metal ion concentration and 10 μM in ligand concentration [12].

https://doi.org/10.1016/j.jinorgbio.2019.01.012
Received 9 October 2018; Received in revised form 18 January 2019; Accepted 20 January 2019
Available online 06 February 2019
0162-0134/

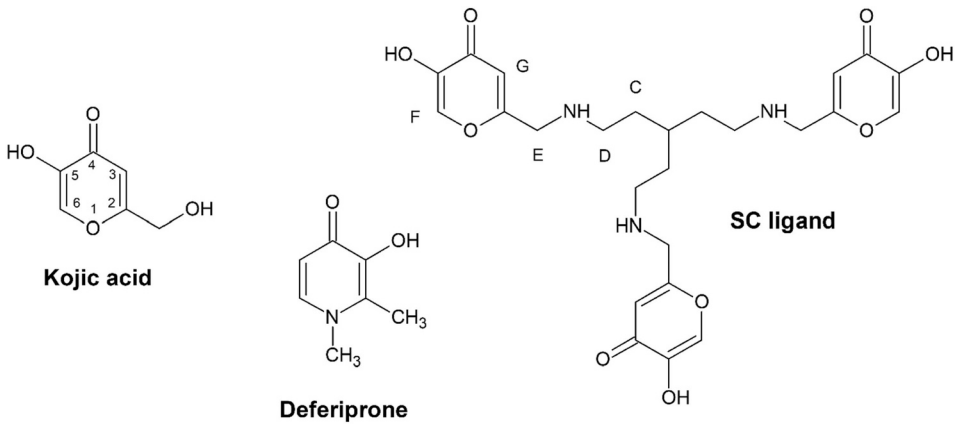

Fig. 1. Molecular structures of kojic acid, deferiprone and of 6,6′,6″-(((nitrilotris(ethane-2,1-diyl))tris(azanediyl))tris(methylene))tris(3-hydroxy-4H-pyran-4-one) (SC ligand). The letters in the structure of SC ligand will be used in NMR attributions.

length, by reacting them with the methylhydroxyl groups in position 2 [10]. The simplicity of synthesis allows an easy and low cost preparation. The different anchoring position of the linker, as well as its length, can affect both protonation and complex formation equilibria. The obtained results remark that the orientation of the oxygen atoms in KA units, related to the anchoring position, strongly affects the protonation constants, while the chelating ability is practically unaffected.

Based on these encouraging results we have explored herein the synthesis of the tripodal KA derivative 6,6′,6″-(((nitrilotris(ethane-2,1-diyl))tris(azanediyl))tris(methylene))tris(3-hydroxy-4H-pyran-4-one), in the following reported as SC ligand, in which three KA units are attached to a tris(2-aminoethyl)amine (tren) backbone.

Potentiometric and spectrophotometric methods, supported by and ^{1}H and ^{13}C NMR spectroscopy and also quantum-mechanical calculations, were thoroughly used to characterize the protonation and the complex formation equilibria with Fe^{3+}, Al^{3+}, Cu^{2+} and Zn^{2+}. Finally, this ligand is bioevaluated for its capacity for metal-mobilization from the body of mice overloaded with Ga^{3+}, and also *in silico* evaluated for its pharmacokinetic properties and druggability [11]. The results are discussed, in comparison with other analogous ligands, in particular the currently marketed chelating drug, Deferiprone (Fig. 1), due to the structural analogy between hydroxypyridinone and hydroxypyrone ligands.

2. Experimental

2.1. Reagents

Kojic acid, tris(2-aminoethyl)amine (tren), NaOH, NaCl, $FeCl_3$, $AlCl_3$, $CuCl_2$, $ZnCl_2$ and HCl were purchased from Aldrich. All the reagents were used without any further purification. Carbonate-free 0.1 M NaOH solution was prepared according Albert and Serjeant [13]. The metal ion standard solutions were prepared by dissolving the required amount of chloride salts in pure double distilled water and adding a stoichiometric amount of HCl to prevent hydrolysis. Fe^{3+} solution was standardized by spectrophotometric analysis using the formation of the colored Fe^{3+}–desferal complex [14], while Al^{3+}, Cu^{2+} and Zn^{2+} solutions were standardized by EDTA titration.

2.2. Synthesis of 6,6′,6″-(((nitrilotris(ethane-2,1-diyl))tris(azanediyl))tris(methylene))tris(3-hydroxy-4H-pyran-4-one)

Kojic acid (1.0 g, 7.04 mmol) was suspended in 20 mL ethanol followed by dropwise addition of tris(2-aminoethyl)amine (350 μL, 2.32 mmol) solved in $CHCl_3$ (2 mL). After stirring the reaction mixture at room temperature for 1 h, the precipitate was filtered and washed with ethyl acetate. The identity and purity of the sample were confirmed by NMR and elemental analysis. Analytical data: 98.5% yield, ^{1}H NMR (D_2O, 500 MHz) δ 2.83 (t, 6H, J = 2.81 Hz), 3.09 (t, 6H, J = 3.09 Hz), 4.49 (s, 6H), 6.49 (s, 3H), 7.82 (s, 3H). ^{13}C NMR (D2O, 500 MHz) δ 39.84, 53.86, 62.92, 112.94, 145.16, 168.24, 184.01, 199.25. Elemental analysis (%) calculated for ($C_{24}H_{36}N_4O_{12}{\cdot}3H_2O$): C 50.35; H 6.34, N 9.79%; found: C 50.53, H 6.21, N 9.72%.

2.3. Potentiometric–spectrophotometric measurements

Potentiometric or combined potentiometric-spectrophotometric measurements for protonation and complex formation equilibria were performed in a thermostatted glass cell equipped with a magnetic stirrer, a Metrohm LL UNITRODE glass electrode connected to a Metrohm 691 pH-meter, a microburet delivery tube connected to a Dosimat 665 Metrohm titrator, an inlet–outlet tube for Argon and a fiber optic dip probe connected to a Varian Cary 50 UV–vis spectrophotometer. Protonation and Fe^{3+} complex formation constants were determined by simultaneous potentiometric and spectrophotometric titrations, while Al^{3+}, Cu^{2+} and Zn^{2+} complex formation constants were potentiometrically determined. Solutions (20 mL at working ligand concentration 5.0×10^{-4} M) were titrated with 0.1 M NaOH at 25.0 °C, and 0.1 M NaCl ionic strength. The electrode was daily calibrated for hydrogen ion concentration by titrating HCl with NaOH in the above experimental conditions and the results were analyzed with Gran procedure [15]. 120 points were generally acquired for each titration. Complex formation studies were performed in triple at 1:1 and 1:2, metal/ligand molar ratios. The reversibility was checked by back titration with HCl in at least one case for each metal/ligand system. Since Fe^{3+} was almost completely complexed when mixing reagents before the base potentiometric titrations, the complex formation equilibria were studied also in strongly acid media (pH 1–3) on sets of solutions at increasing concentrations of HCl until the disappearance of the bands of complexed iron. These measurements were made in batch adjusting the ionic strength by proper additions of HCl and NaCl.

Combined potentiometric spectrophotometric measurements were done in the 200–400 nm spectral range for protonation equilibria, and in the 400–800 nm range for Fe^{3+} complexation, using 0.2 and 1 cm path lengths respectively. Protonation and complex formation data were analyzed using Hyperquad2013 [16] and HypSpec [17] programs. Log β_{pqr} values refer to the overall equilibria $pM + qH + rL \leftrightarrows M_pH_qL_r$ (electrical charges omitted). The hydrolysis constant at 25 °C and 0.1 M ionic strength used in the refinement procedure are reported in Table 1S.

2.4. NMR spectroscopy

Nuclear Magnetic Resonance (NMR) experiments were carried out

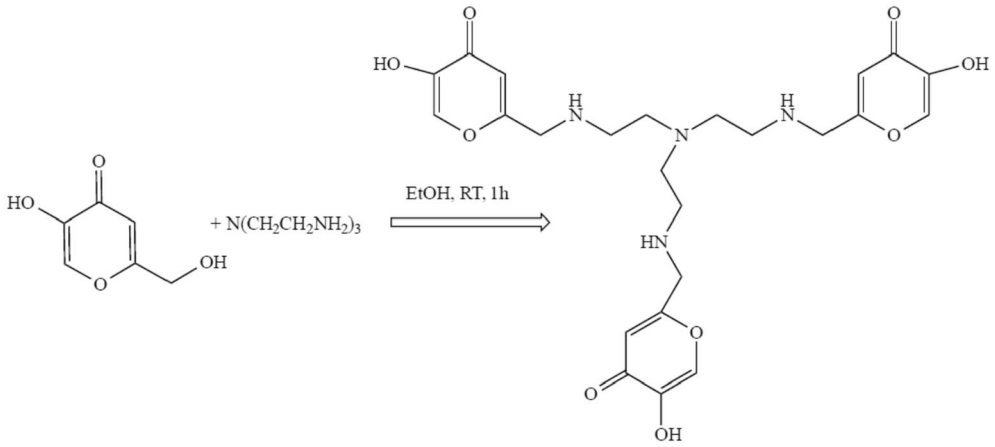

Scheme 1. Scheme of the synthesis of ligand SC starting from KA and tren.

by using a Bruker AscendTM 400 MHz spectrometer equipped with a 5 mm automated tuning and matching broad band probe (BBFO) with z-gradients, as previously described [18–20]. Ligand concentrations varied in the range 2–5 mM, in 90/10 (v/v) H2O/D2O at 298 K using 5 mm NMR tubes. 2D $^{1}H-^{13}C$ HSQC spectra (Heteronuclear Single Quantum Coherence) were acquired using a phase-sensitive sequence employing Echo-Antiecho-TPPI gradient with a heteronuclear coupling constant JXH = 145 Hz, and shaped pulses for all 180° pulses on f2 channel with decoupling during acquisition. Sensitivity improvement and gradients in back inept were also used. 2 s and 90° pulses of about 10 μs were employed as relaxation delays of in all the measurements. The suppression of the solvent was performed in 1D ^{1}H and 2D $^{1}H-^{1}H$ TOCSY (Total Correlation Spectroscopy) experiments by using excitation sculpting with gradients. The spin-lock mixing time of TOCSY experiments was obtained with MLEV17. $^{1}H-^{1}H$ TOCSY spectra were performed using mixing times of 60 ms. A combination of 1D, 2D TOCSY, HSQC experiments was used to assign the signals of both free and metal-bound ligands at different pH values. All NMR data were processed with TopSpin (Bruker Instruments) software and analyzed by Sparky 3.11 and MestRe Nova 6.0.2 (Mestrelab Research S.L.) programs.

2.5. Molecular modelling studies

Density functional theory (DFT) calculations were carried out on the complexes and ligands using the three-parameter hybrid functional B3LYP [21,22] as also previously done for similar systems [23–27]. The LANL2DZ ECP has employed for the metal ions [28], while other elements were treated using a 6–31 + G (25) Gaussian-type basis set. Geometry search for the large Fe_3S_3 complex has been performed at semiempirical (PM6) level. All calculations were carried out using the Gaussian16 program [29]. The TD-DFT spectra of the Fe^{3+} complexes were calculated with the B3LYP functional at the coordinates of the minimum previously obtained using the def2-TZVP basis set for all elements [30]. The latter calculations were performed using ORCA 4.0 [31].

2.6. Biodistribution studies

^{67}Ga-citrate injection solution was prepared by dilution of ^{67}Ga citrate from Mallinckrodt Medical B.V. with saline to obtain a final radioactive concentration of approximately 5–7 MBq/100 μL. Biodistribution studies were carried out in groups of 3 female CD1 mice (randomly bred, Charles River, from CRIFFA, France) weighing *ca.* 25 g. Mice were intravenously (i.v.) injected with 100 μL (5.5 MBq) of ^{67}Ga citrate *via* the tail vein immediately followed by intraperitoneal (i.p.) injection of 0.5 μmol of the ligand in 100 μL saline. Animals were maintained on normal diet *ad libitum* and were sacrificed by cervical dislocation at 15 min, 1 h and 24 h post-administration. The administered radioactive dose and the radioactivity in sacrificed animals were measured in a dose calibrator (Capintec CRC25R). The difference between the radioactivity in the injected and sacrificed animal was assumed to be due to whole body excretion. Tissue samples of main organs were then removed for counting in a gamma counter (Berthold LB2111, Berthold Technologies, Germany). Biodistribution results were expressed as percent of injected activity per organ (% I.A.) and as percent of injected activity per gram of organ (%I.A./g) and presented as mean values ± standard deviation. Biodistribution data were evaluated by an analysis of variance. The level of significance was set at 0.05 (two-sided). Animal studies were carried out under the supervision of experienced researchers in animal facilities approved by the national authorities according to the national and European laws.

3. Results and discussion

3.1. Synthesis and characterization

The tripodal chelator SC was designed to contain three KA coordinating groups attached to a tris(2-aminoethyl)amine skeleton (Fig. 1). The ligand was synthesized through the straightforward method outlined in Scheme 1 and detailed in the experimental section, with a 98.5% yield.

The easy and cheap synthesis has to be remarked, together with the extremely high yield. The length of the linker chains between the apical tertiary nitrogen atom and the KA chelating moieties was based on the assumption that it was long enough to allow the wrapping of the metal ion by the KA moieties. A short linker, by reducing the molecular weight of the ligand, could represent a benefit for both the membrane crossing and for the accessibility to cytoplasmic iron pools [32].

3.2. Protonation equilibria

SC ligand is characterized by six protonation sites, the three O– groups in the KA units and the three amino groups of the tren backbone. Potentiometric-spectrophotometric titrations were performed in the 240–370 nm wavelength range (Figs. 1S and 2S), with the aim of evaluating the protonation constants and attributing each protonation step to a given basic group on the molecule (amine or O- groups). The resulting data, processed with HypSpec program [17] allowed the calculation of the six protonation constants in Table 1 and of the absorptivity spectra of the seven differently protonated species in Fig. 2. These spectra permit to ascribe the three last protonation steps with log K 8.04, 7.70 and 7.10 to the O^{-} group in the KA units. In fact, ligand SC, in its completely protonated form LH_6^{3+}, is characterized by a band at

Table 1
Protonation constants of the ligand SC (log β and log K) at 25 °C and 0.1 M NaCl ionic strength[a]. The protonation constants (log K) of tren in the same experimental conditions are from Reference [33].

SC ligand			tren	
Formed species	log β	log K	Formed species	log K
SCH^{2-}	10.18(2)	10.18	TH^{+}	10.08
SCH_2^{-}	19.83(1)	9.65	TH_2^{2+}	9.55
SCH_3	28.55(1)	8.72	TH_3^{3+}	8.41
SCH_4^{+}	36.59(1)	8.04[b]		
SCH_5^{2+}	44.29(1)	7.70[b]		
SCH_6^{3+}	51.39(1)	7.10[b]		

[a] The protonation constant of KA in the same conditions is 7.70 [9].
[b] Protonation of KA unit.

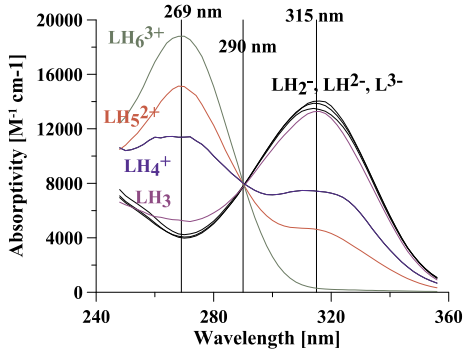

Fig. 2. Absorptivity spectra of the variously protonated forms of SC ligand, calculated using HypSpec program [17].

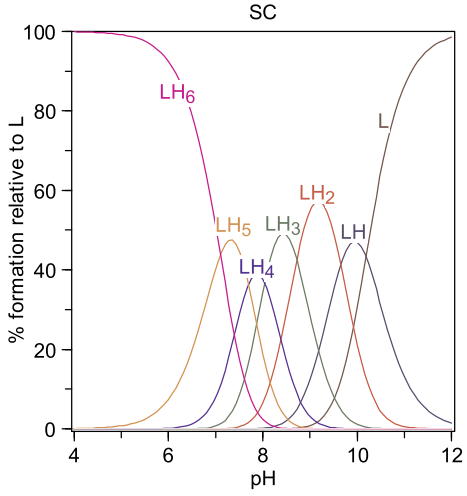

Fig. 3. Speciation plot of SC ligand, calculated using Hyss program [34].

269 nm similar in position to the band of protonated KA, but more intense due to the contribution of three similar chromophore units. Passing to the penta-protonated form LH_5^{2+}, the band at 269 nm decreases in intensity and a new band appears at 315 nm, as in the case of the dissociation of KA. In the second and third dissociation step, until the formation of the neutral LH_3 species, the band at 269 nm decreases and the band at 315 nm reaches its maximum value $\varepsilon = 13{,}000\ M^{-1}\ cm^{-1}$. Fig. 3 presents the speciation plots of SC ligand.

The three following deprotonation steps do not present appreciable spectral variations. Based on the above observations, the first three deprotonation steps were attributed to the dissociation of the OH groups in the KA moieties, and the following three, spectrally silent, to that of the charged amino groups. NMR results support the above conclusions. The ^1H and ^1H-^{13}C-HSQC NMR spectra with the assignments of all the protons of ligand SC are reported in Fig. 4.

The ligand shows a very high symmetry in our NMR conditions; indeed, the three KA units, joined by a tris(2-aminoethyl)amine (tren) backbone, give a unique ^1H and ^{13}C pattern. In Fig. 5 the ^1H NMR spectra as a function of the pH in the range 2.60–9.90 are reported. Table 2S displays ^1H and ^{13}C resonance assignments of SC ligand by changing the pH.

The variation in chemical shifts, which starts to appear from pH 6.5 on, points to high field for all the protons, indicating the deprotonation of the nearby sites by raising the pH. As showed in the plot in Fig. 6 the most affected protons are the following in the order F > C = D = G > E from pH 7.10 on. From pH 7.10 on, the observed shifts of C, D and E protons can support the deprotonation of the NH_2^{+} sites on the linker.

On the other hand, the change in chemical shifts of the ^{13}C signals reported in the plot in Fig. 7 shows that it pointed toward low field for all the carbons except for G nucleus.

3.3. Iron complex formation equilibria

The complex formation equilibria between Fe^{3+} and SC ligand were studied by a combined potentiometric-spectrophotometric procedure, previously discussed [10]. Furthermore, since Fe^{3+} is almost completely complexed when mixing reagents before the base potentiometric titration, the complex formation equilibria were studied also in strong acidic solutions (pH 0.4–2) on sets of solutions at increasing concentrations of HCl until the disappearance of the bands of complexed iron. These measurements at acidic pH values were made in batch adjusting the ionic strength by proper additions of HCl and NaCl. In the case of four solutions at pH between 0.4 and 0.9 the ionic strength was not 0.1, but determined by the HCl concentration (these points were not taken into account in the calculations). Combined potentiometric-spectrophotometric measurements were done in the 350–700 nm range, using 1 cm path lengths. Some representative spectra collected with both procedures at the same concentration of reagents in a 1:1 ratio are reported in Fig. 3Sb and c. Complex formation data were analyzed using Hyperquad [16] and HypSpec [17] programs. The complex formation constants so evaluated are reported in Table 2, and the related speciation plot in Fig. 8.

As can be seen from the speciation plot, starting from pH = 1 the formation of $[Fe(SC)H_5]^{5+}$, and almost simultaneously of $[Fe(SC)H_4]^{4+}$ is apparent. The first is characterized by a visible band centered at 500 nm, that shifts at 475 nm and increases in intensity with the formation of $[Fe(SC)H_4]^{4+}$. After pH 3 a third species $[Fe(SC)H_3]^{3+}$ appears whose main band is centered at 397 nm. The similarity of the spectral variations with those observed on the system Fe^{3+}/KA, during the formation of the species $[Fe(KA)]^{2+}$, $[Fe(KA)_2]^{+}$ and $Fe(KA)_3$ [9] (Fig. 3Sa), lead to attribute $[Fe(SC)H_5]^{5+}$ to a complex in which Fe^{3+} is coordinated by one KA unit of SC, $[Fe(SC)H_4]^{4+}$ by two KA units, and $[Fe(SC)H_3]^{3+}$ by all the three KA units. The DFT calculations later presented do not support this last interpretation, and $[Fe(SC)H_3]^{3+}$ should be presumably a polynuclear complex with the same Fe:SC molar ratio. A possible structure of the M:SC 3:3 (where Fe3+ is replaced by Al3+ for simplicity) is reported in Fig. 4S: in this case it is shown that 2 metal ions are completely coordinated by the KA moieties while the third metal ion is bound by two units. Unfortunately, the low melting temperature of ligand SC prevented performing ESI-MS measurements. In the $[Fe(SC)H_3]^{3+}$ complexes, or similar polynuclear complexes, all the nitrogen atoms are protonated. This complex then loses five protons with pK 7.50, 8.62 (two protons), 9.31 and 9.79. The decrease of the intensity of the visible bands from pH 6.70 on (Fig. 3Sc) presumably is indicative of the formation of hydroxo complexes during the first deprotonations where Fe^{3+} is coordinated by only two KA units, and the charged nitrogen atoms then lose their protons in the following steps.

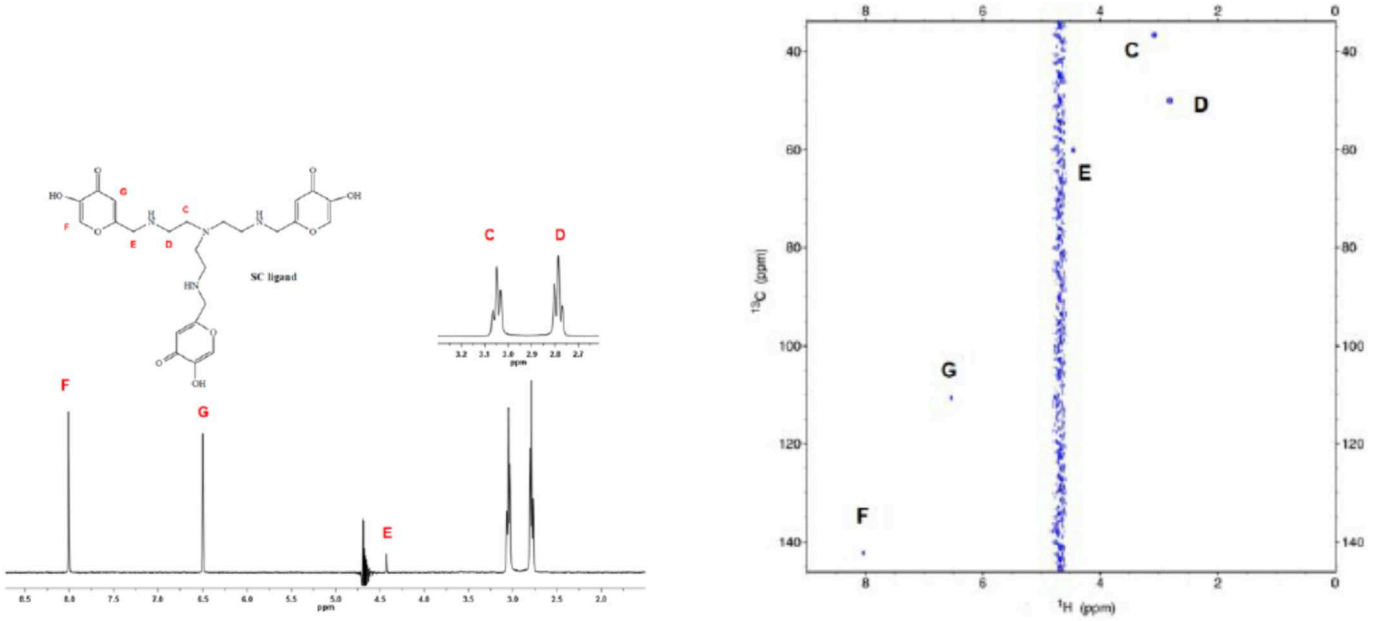

Fig. 4. ^{1}H (left) and ^{1}H-^{13}C-HSQC (right) NMR spectra with the assignments of all the signals.

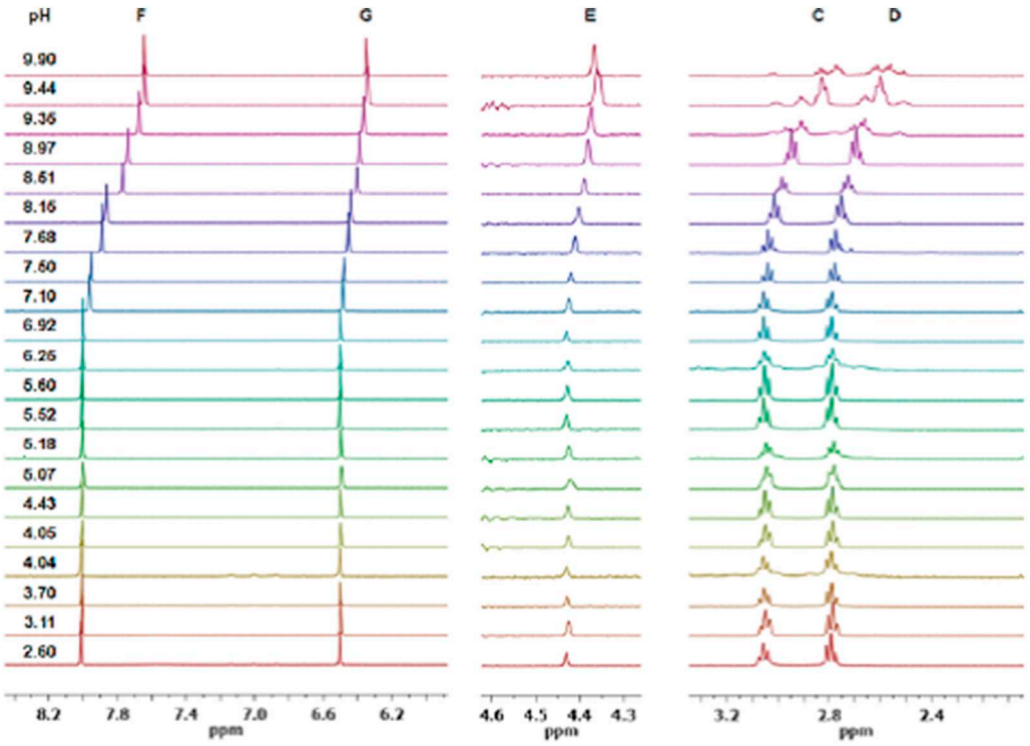

Fig. 5. ^{1}H NMR spectra as a function of pH in the pH range 2.60–9.90.

The complex formation equilibria of the ligand with Fe^{3+} ions were studied also by NMR technique. However, because of the low stability of Fe^{3+} solutions during the experimental condition used for NMR measurements and some broad signals obtained with this system, Ga^{3+} ions were used instead of Fe^{3+} ions as an amenable diamagnetic probe in the NMR measurements.

^{1}H NMR spectra as a function of pH, in the range 3.10–9.60 using a 3:2 SC:Ga^{3+} molar ratio, are reported in Fig. 9.

The ^{1}H chemical shift δΔ variations for the SC:Ga^{3+} and SC:Al^{3+} in a 1:1 molar ratio *versus* SC free ligand by changing the pH are reported in Fig. 10. These plots give evidence of the similar behavior of the two metal ions.

In fact, the behavior of the Ga^{3+}-SC (and presumably Fe^{3+}-SC) system by changing the pH is widely comparable to that of the Al^{3+}-SC system, evidently showing the involvement of the oxygen atoms from the three aromatic rings and the non-involvement of the nitrogen atoms from the linker. At the same time, at pH higher than 8, the signals from the free ligand strongly reappear. The species indicated as FeL in the speciation plot, should be some hydroxylate species, following the NMR behavior where the signals of the free ligands very clearly reappeared at pH higher than 8.

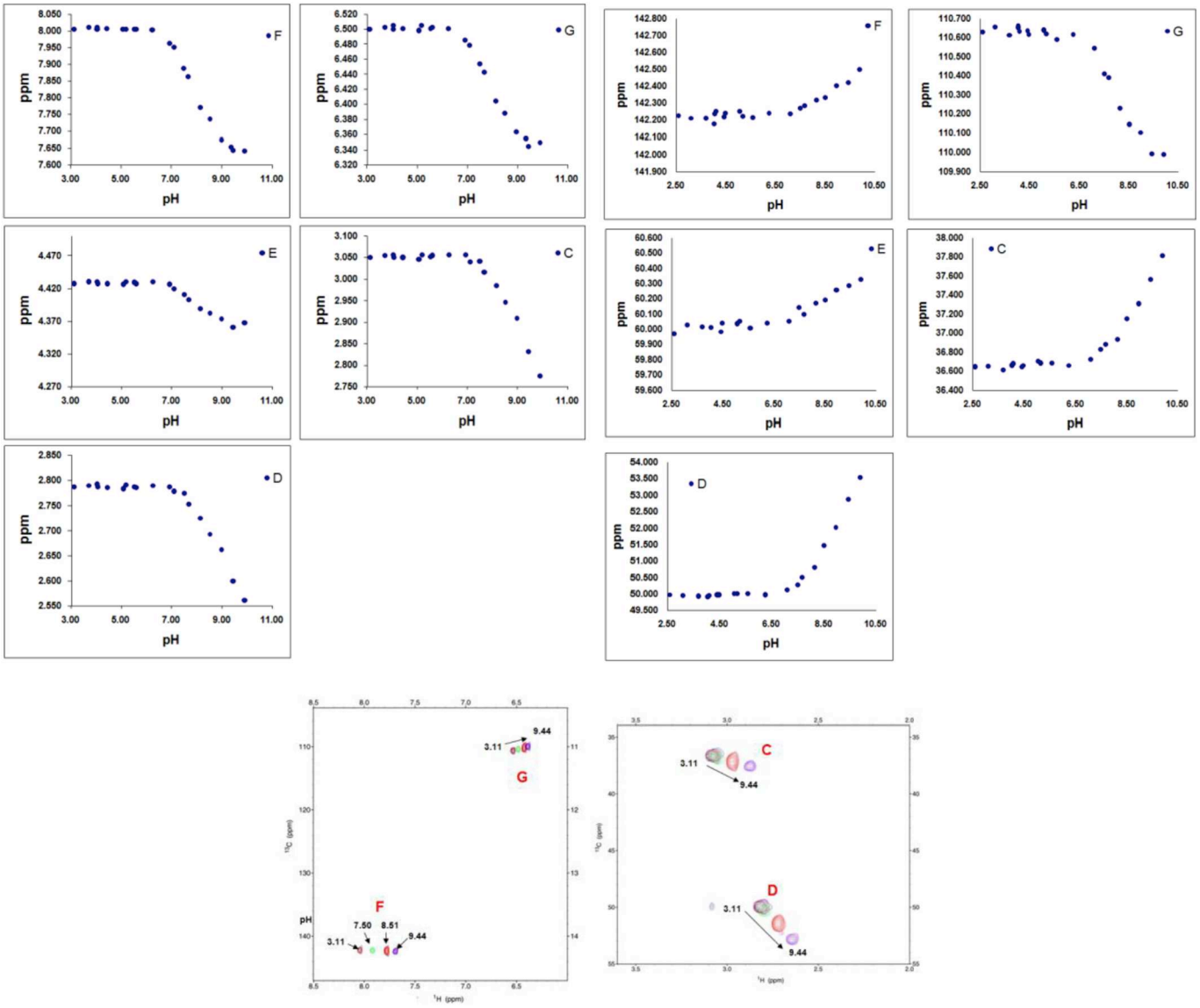

Fig. 6. Trend of ^{1}H and ^{13}C chemical shifts *vs* pH, and some ^{1}H-^{13}C-HSQC spectra at selected pH values.

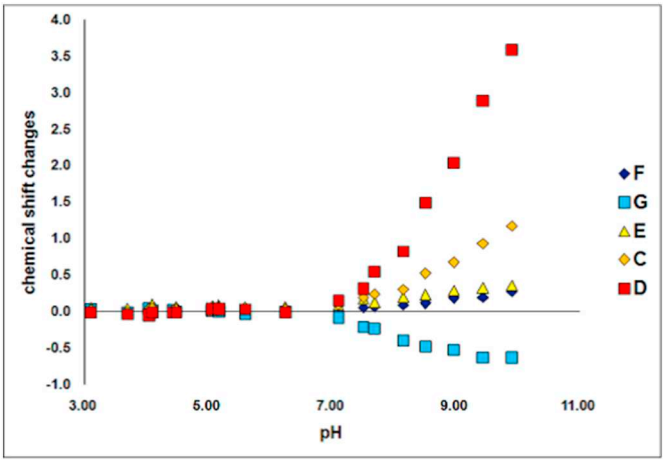

Fig. 7. Trend of ^{13}C chemical shifts *vs* pH.

Table 2
Complex formation constants of the system Fe^{3+}/SC at 25 °C and 0.1 M NaCl ionic strength, calculated with HypSpec program [17].

Formed species	Log β	pK
$[Fe(SC)H_5]^{5+}$	53.5(6)	1.4
$[Fe(SC)H_4]^{4+}$	52.12(7)	4.00
$[Fe(SC)H_3]^{3+}$	48.12(4)	7.50
$[Fe(SC)H_2]^{2+}$	40.62(4)	8.62
Fe(SC)	23.37(5)	9.31
$[Fe(SC)H^{-1}]$	14.06(3)	9.79
$[Fe(SC)H_{-2}]^{2-}$	4.27(4)	–
pFe	**19.5**	

3.4. Aluminium complex formation equilibria

The complex formation equilibria involving Al^{3+} and SC ligand were studied by potentiometric titrations. The formed complexes and the related stability constants are reported in Table 3, and the related

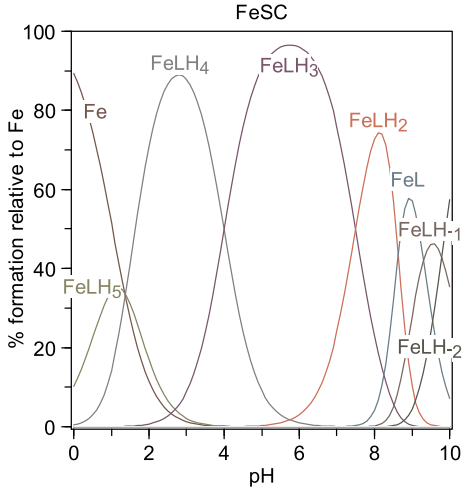

Fig. 8. Speciation plot of the system Fe^{3+}/SC, at $C_{Fe3+} = C_{SC} = 1$ mM, calculated using Hyss program [34].

speciation plots in Fig. 11. The mechanism of complexation resembles that one of iron, though with lower stability constants. A complex $[Al(SC)H_5]^{5+}$ forms from pH 3 on, in which the metal ion is coordinated by one KA unit; almost simultaneously the second $[Al(SC)H_4]^{4+}$ species forms, with Al^{3+} ion coordinated by two KA units. Finally, from pH 5 on starts the formation of complex $[Al(SC)H_3]^{3+}$ fully coordinated by three KA units, till protonated on the nitrogen atoms. Two of these charged nitrogen atoms lose their protons with pK 8.10 and 8.63, almost one p*K* unit lower than for pure SC ligand, coming from the effect of the higher total positive charge of the molecule. The obtained pAl value is 5.8 units lower than that with iron, in line with the normal behavior of oxygen-based ligands with these two trivalent metal ions.

The complex formation equilibria of the ligand with Al^{3+} ions were also studied by NMR titrations. ^{1}H NMR spectra are reported in Fig. 12 as a function of the pH in the range 3.07–9.46 at a 1:1 SC:Al^{3+} molar ratio.

Starting from pH 3 a new signal is visible, though together with the signals of the free ligand, showing that the complexes start anyway to form at acidic pH. A further new signal is clearly visible at pH 3.79,

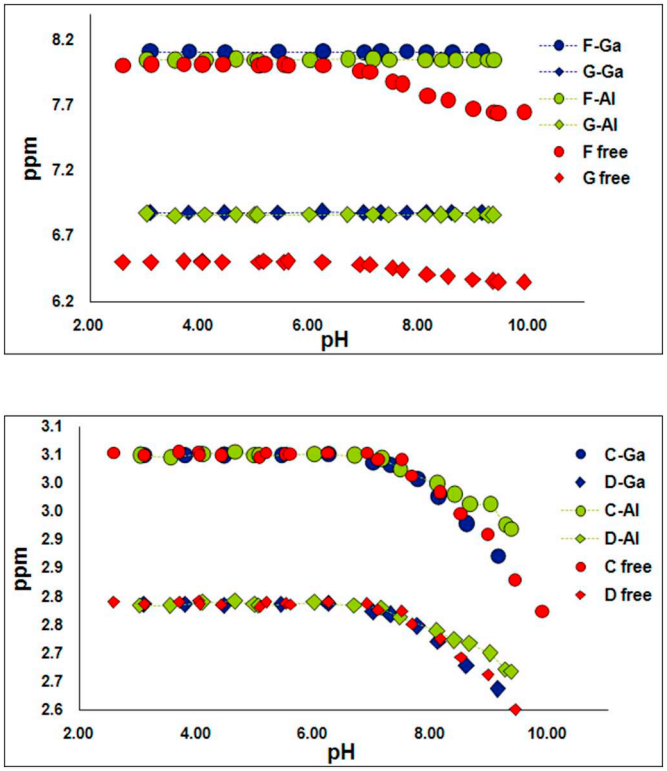

Fig. 10. ^{1}H Chemical shift variation for the SC:Ga and SC:Al (1:1) systems *vs* that of SC free with changing pH.

though in a low concentration, together with another one that reaches its maximum around pH 8 and appears as the most important species. At pH higher than 8, this species decreases in intensity while the signals of the free ligand appear more intense suggesting that, at high pH, Al^{3+} ions can be rather involved in the formation of some hydrolytic (mixed ligand-hydroxo) metal complex species.

The formation of Al^{3+}-SC complexes involves the oxygen atoms from the aromatic rings, while nitrogen atoms from the linker are not involved in the interaction with Al^{3+} ions. In fact, the most affected

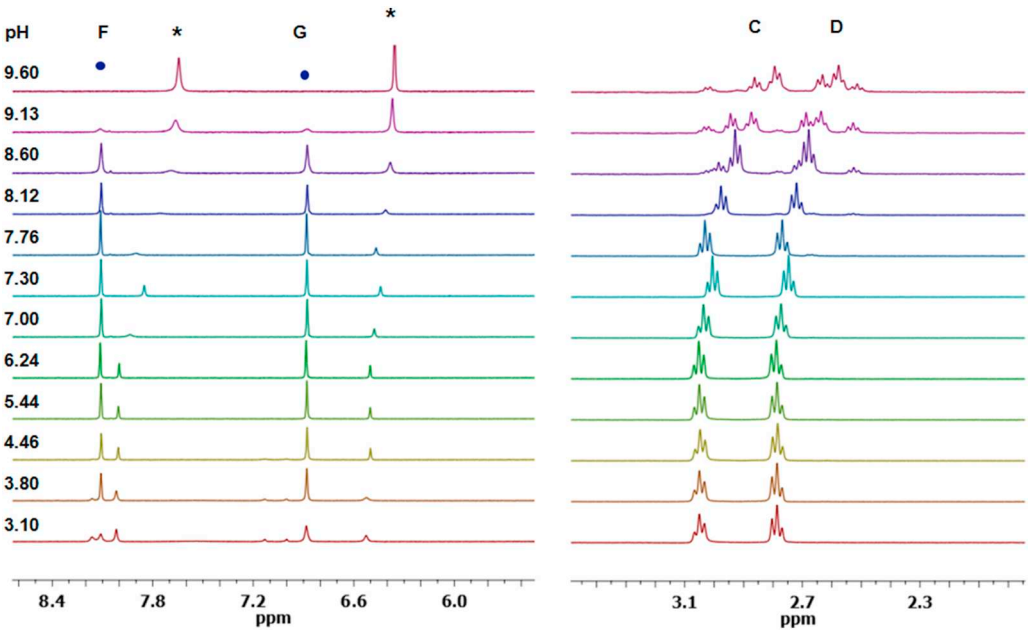

Fig. 9. ^{1}H NMR spectra as a function of the pH in the range 3.10–9.60 in a 3:2 SC:Ga^{3+} molar ratio. Circles indicate the complexes, asterisks the free ligand.

Table 3
Complex formation constants of the system Al^{3+}/SC at 25 °C and 0.1 M NaCl ionic strength, calculated with Hyperquad program [16].

Formed species	Log β	pK
$[Al(SC)H_5]^{5+}$	51.72(2)	3.64
$[Al(SC)H_4]^{4+}$	48.08(1)	5.63
$[Al(SC)H_3]^{3+}$	42.45(1)	8.10
$[Al(SC)H_2]^{2+}$	34.35(2)	8.63
$[Al(SC)H]^{+}$	25.72(3)	–
pAl	**13.7**	

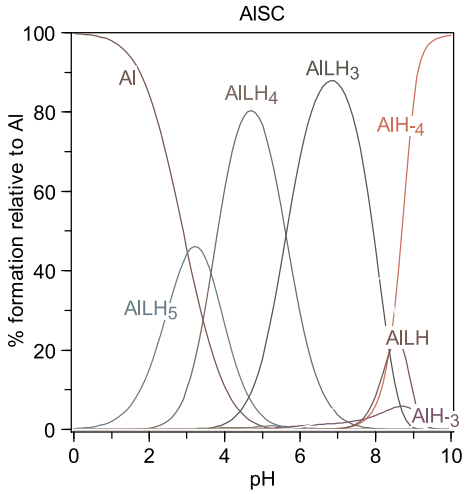

Fig. 11. Speciation plot of the system Al^{3+}/SC ligand, at $[Al^{3+}] = [SC] = 1$ mM, calculated using Hyss program [34].

protons appear to be those on the aromatic rings, mainly F and G protons. The chemical shift values of F and G protons of the Al^{3+}-SC species appear constant in all the range of pH supporting that one predominant species is present in a slow exchange in the NMR scale. The complexed species appears highly symmetric suggesting that all the three aromatic rings are involved in the coordination.

Only one signal is visible for each group of protons indicating that a relevant interaction between the metal ion and SC ligand is present especially in the range of pH from 6 to 8.

Starting at pH higher than 8 several signals appear for the groups of protons suggesting that aluminium ions are, mostly not more coordinated to the SC ligand. The species indicated as AlSH in the speciation potentiometric plot, should be a hydroxylate species, following the NMR behavior where the signals of the free ligands very clearly reappeared at pH higher than 8.

In Fig. 5S the ^{1}H and ^{13}C δΔ chemical shift variation for F, G, C and D protons for SC:Al^{3+} system at 1:1 molar ratio by changing the pH are reported, and in Table 3S the ^{1}H and ^{13}C resonance assignments at variable pH.

Table 4
Complex formation constants of the system Cu^{2+}/SC at 25 °C and 0.1 M NaCl ionic strength, calculated with Hyperquad program [16].

Formed species	Log β	pK
$[Cu(SC)H_4]^{3+}$	46.83(2)	3.92
$[Cu(SC)H_3]^{2+}$	42.91(1)	7.26
$[Cu(SC)H_2]^{+}$	35.65(2)	7.53
Cu(SC)H	28.12(1)	8.07
$[Cu(SC)]^{-}$	20.05(2)	9.55
$[Cu(SC)H_{-1}]^{2-}$	10.50(2)	
pCu	**14.6**	

3.5. Copper complex formation equilibria

The complex formation equilibria between Cu^{2+} and ligand SC were studied by potentiometric titrations. The formed complexes and the related stability constants are reported in Table 4, and the speciation plot in Fig. 13. Even if the complexation mechanism resembles that with iron and aluminium ions, a completely different situation is present. The first formed species $[Cu(SC)H_4]^{3+}$ is a complex with Cu^{2+} coordinated by two nitrogen atoms. This transforms in $[Cu(SC)H_3]^{2+}$ at pK 3.92 with Cu^{2+} coordinated by all the three nitrogen atoms, analogously to what observed with tren (T) (Table 5 and Fig. 13) [33]. The three remaining protons, lost with pK values almost the same of that measured for the three KA units in pure SC ligand, confirm the above attributions, as well as the similar values of pCu for SC and tren, slightly higher the former.

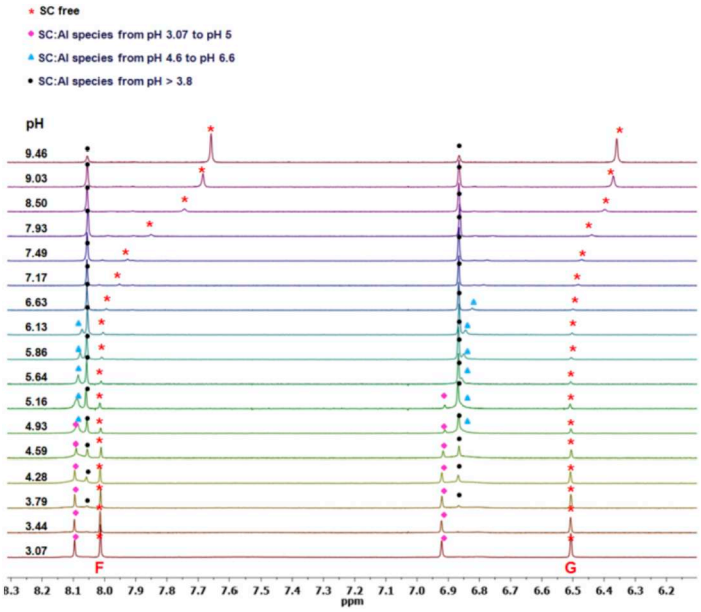

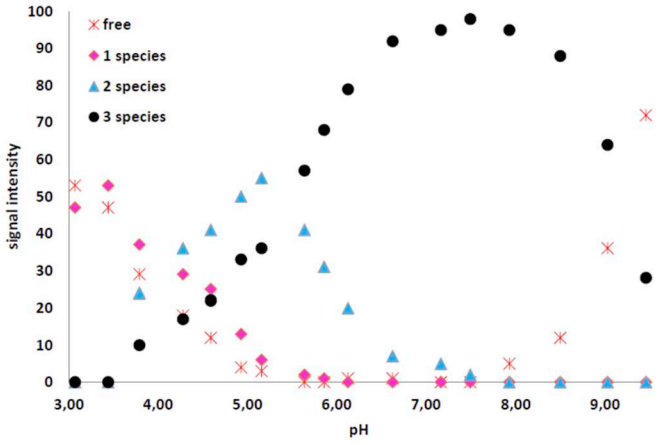

Fig. 12. Left, ^{1}H NMR as a function of the pH in the range 3.03–9.35 in a 1:1 SC:Al^{3+} molar ratio, at SC concentration 2 mM. On the right, the percentage of the different SC species *vs* pH.

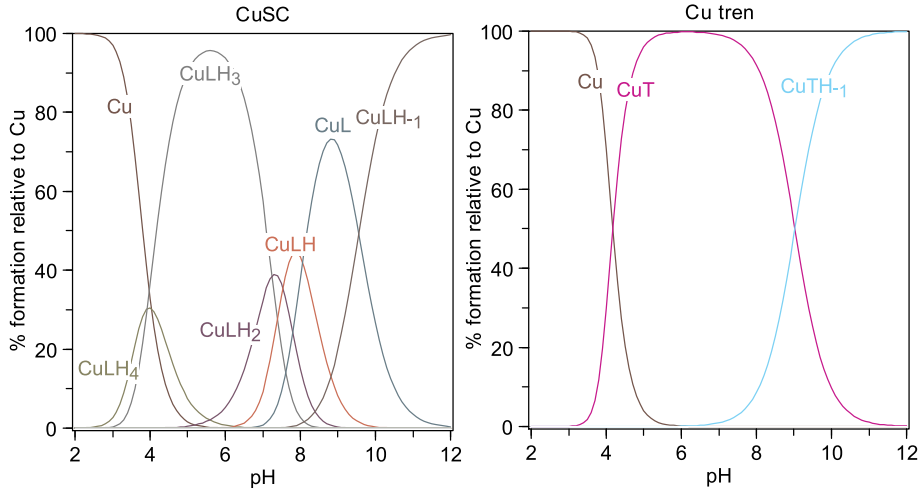

Fig. 13. Speciation plot of the systems left) Cu^{2+}/SC, at $[Cu^{2+}] = [SC] = 1$ mM, right) Cu^{2+}/tren, at $[Cu^{2+}] = [tren] = 1$ mM, calculated using Hyss program [34]; tren = T.

Table 5
Complex formation constants of tren (T) with Cu^{2+} and Zn^{2+} at 25 °C and 0.1 NaCl M ionic strength [33].

Formed Species	Cu^{2+}	Zn^{2+}
	log β	log β
MT	18.83(1)	14.40(2)
MTH_{-1}	9.80(1)	4.09(3)
pM	13.9	9.5

^{1}H NMR studies for SC-Cu^{2+} system using sub-stoichiometric amounts of Cu^{2+} ions, due to its paramagnetic behavior, have been carried out. In Fig. 14 the NMR titration of SC ligand with increasing additions of sub-stoichiometric amounts of Cu^{2+} ions at pH 7.10, from 200:1 to 1:1 SC: Cu^{2+}molar ratio, is reported. The most affected protons are, in this case, F protons from the aromatic ring, while G from the aromatic ring and C and D protons from the linker remain unchanged till 1:1 molar ratio, where a disappearance of all the signals is visible.

The NMR spectra at 1:1 SC: Cu^{2+}molar ratio at variable pH values are reported in Fig. 15. It is possible to see that whereas C and D protons are still visible since acidic pH, F and G protons disappear. The disappearance of all the signals happen at pH 4.5 and thus, for that reason, the involvement of the nitrogen atoms cannot be demonstrated, but also cannot be excluded by looking to the NMR results only, as clearly visible from the NMR titration analysis obtained by changing the pH from 3.1 to 7.1 for SC:Cu^{2+} 1:1 molar ratio system.

3.6. Zinc complex formation equilibria

The complex formation equilibria between Zn^{2+} and ligand SC were studied by potentiometric titrations. The formed complexes and the related stability constants are reported in Table 6, and the speciation plot in Fig. 16. The results with Zn^{2+} are unexpected, and the pZn value is quite high. Surely, a simple coordination scheme through KA units as with the trivalent metal ions cannot be considered, but rather through

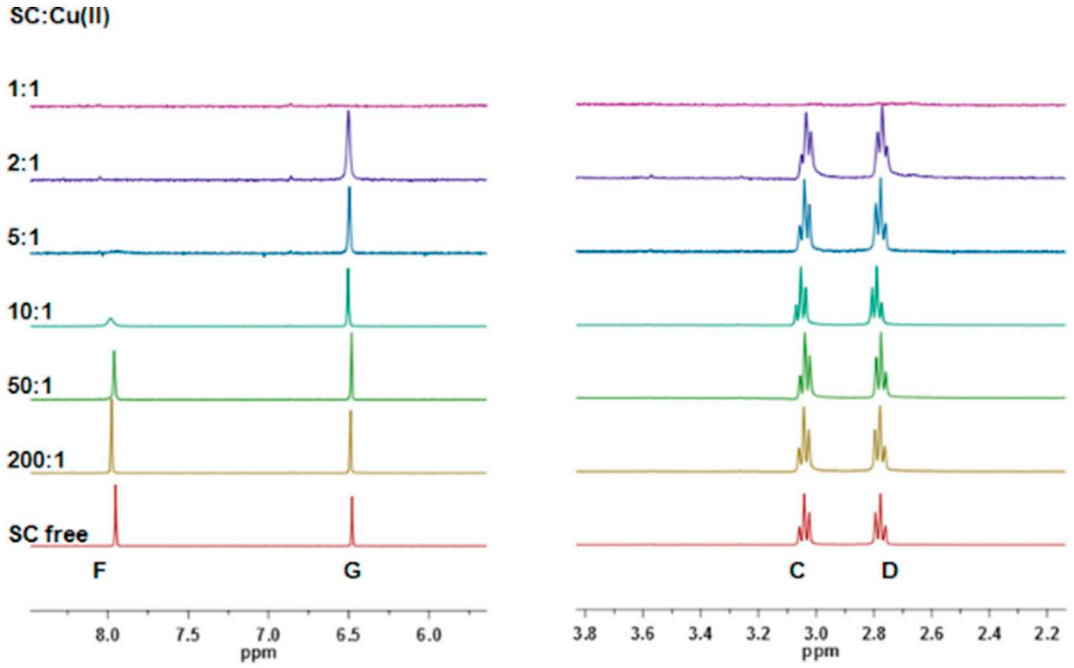

Fig. 14. ^{1}H NMR titration of SC ligand with increasing additions of sub-stoichiometric amounts of Cu^{2+} ions at pH 7.10, from 200:1 to 1:1 SC:Cu^{2+}molar ratios.

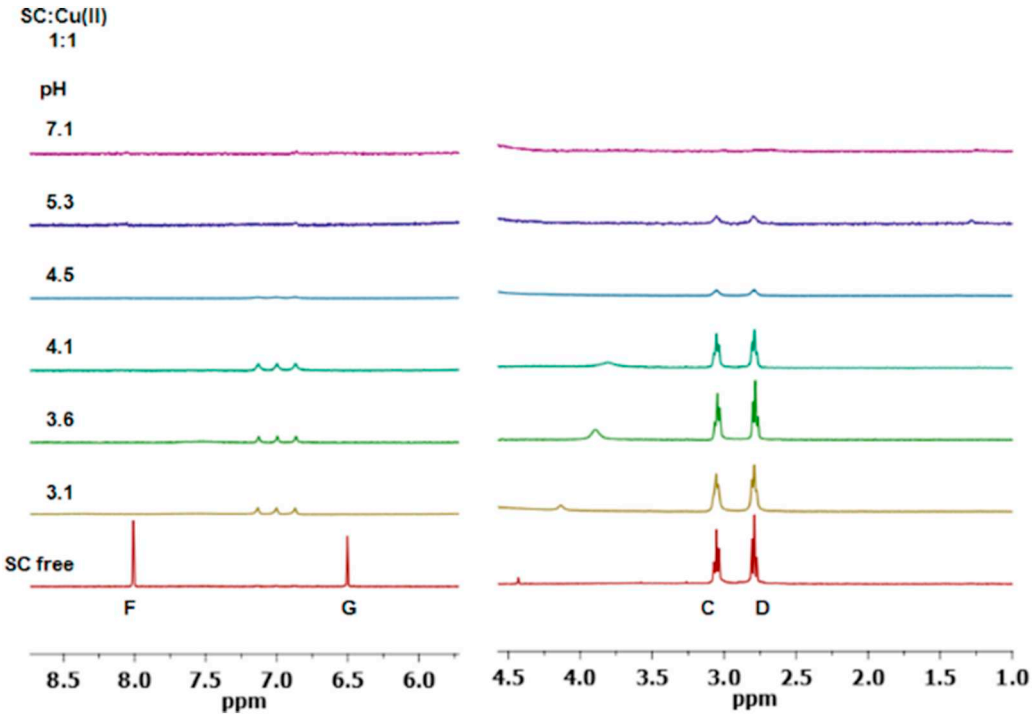

Fig. 15. ^{1}H NMR spectra at 1:1 SC: Cu^{2+} molar ratio at pH values variable from 3.1 to 7.1.

Table 6
Complex formation constants of the system Zn^{2+}/SC at 25 °C and 0.1 M NaCl ionic strength, calculated with Hyperquad program [16].

Formed species	log β	pK
$[Zn(SC)H_4]^{3+}$	43.88(1)	5.24
$[Zn(SC)H_3]^{2+}$	38.64(5)	6.14
$[Zn(SC)H_2]^{+}$	32.50(1)	7.43
Zn(SC)H	25.07(1)	7.89
$[Zn(SC)]^{-}$	17.18(1)	10.27
$[Zn(SC)H_{-1}]^{-}$	6.91(1)	
pZn	**11.4**	

nitrogen atoms as in the case of Cu^{2+}. NMR measurements have been used to have an insight on the coordination behavior of Zn^{2+} ions toward SC ligand.

The ^{1}H NMR spectra for the system SC:Zn^{2+} at 1:1 molar ratio, and at pH values from 3.72 to 9.74, are reported in Fig. 17.

In Fig. 18: a) ^{1}H NMR spectrum for the system SC:Zn^{2+} at 1:1 molar ratio at pH 7, and b) ^{1}H-^{13}C-HSQC NMR spectra for the system SC:Zn^{2+} 1:1 molar ratio at different pH values are reported. By the NMR analysis, the proton signals appear with a fast exchange in the NMR scale, as it typically happens for Zn^{2+} systems. In this case, differently from the coordination behavior of the trivalent Al^{3+} and Ga^{3+} ions with SC ligand, the most affected protons are C and D protons from the linker, which shift to higher fields, suggesting the involvement of the nitrogen atoms in the coordination to Zn^{2+} ions. On the other hand, F and G protons are not influenced, unless at higher pH. We also note that E protons are less affected than C and D protons by the addition of Zn^{2+} ions, supporting the idea that only one major species is formed, where the C nucleus is the most affected by the interaction of Zn^{2+} ions with

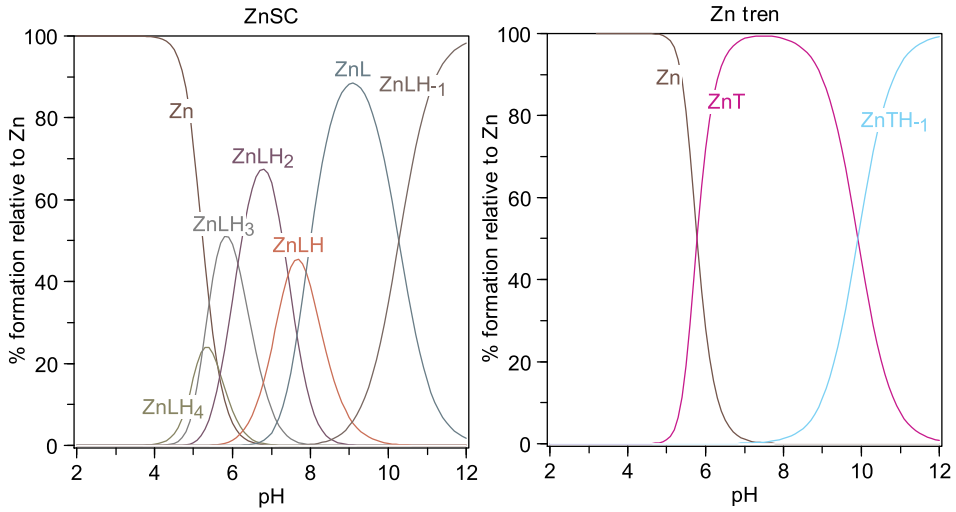

Fig. 16. Speciation plot of the systems left) Zn^{2+}/SC, at [Zn^{2+}] = [SC] = 1 mM, right) Zn^{2+}/tren, at [Zn^{2+}] = [tren] = 1 mM, calculated using Hyss program [34]; tren = T.

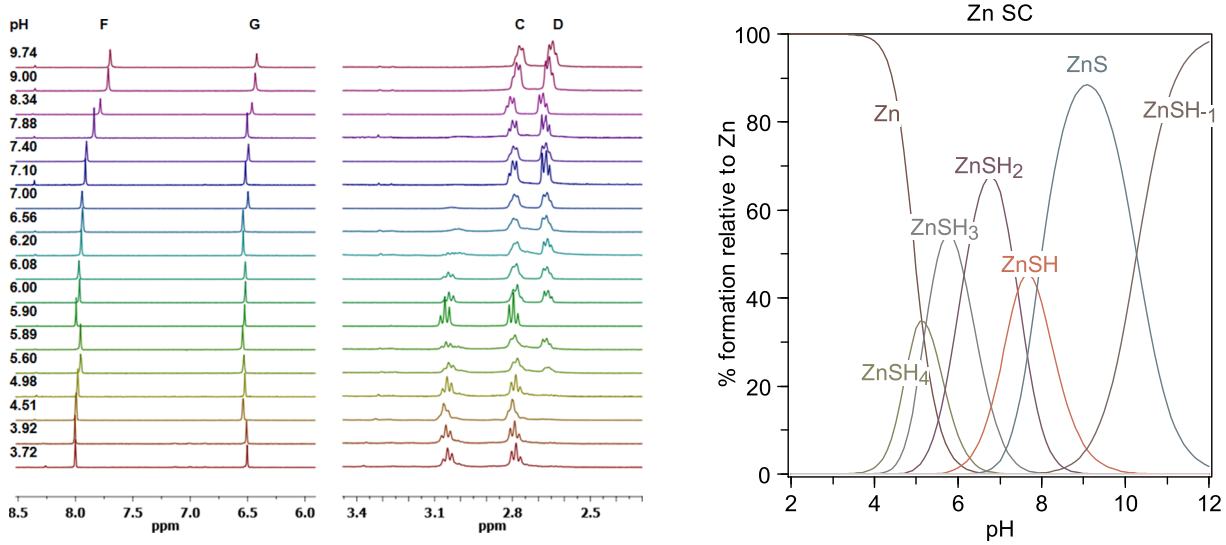

Fig. 17. ^{1}H NMR spectra for the system SC:Zn^{2+} at [SC] = [Zn^{2+}] = 5 mM, at pH values from pH 3.72 to 9.74; on the right the speciation plot at the same concentrations.

SC ligand, following the order C ≫ D ≫ E.

No evidences is found in the NMR results about the possible involvement of the donor atoms on the aromatic rings, unless a very small chemical shifts variation, which can depend from a general different electronic environment after the Zn^{2+} coordination. In agreement with the involvement of the nitrogen donor atoms, the coordination starts at pH higher than 5.9, differently from the starting coordination pH evidenced for Al^{3+}, Ga^{3+}. At pH 7.4 the formation of the species with the higher δΔ values is noted. It is noteworthy that at pH higher than 8, a new species is also visible, though the very low shifts suggest the formation of a species very similar regarding the stoichiometry and the coordination environment of Zn^{2+} ions, but with some differences related to a different protonation state of the SC ligand.

In Fig. 6S the NMR plots for ^{1}H chemical shift δΔ variations for the SC:Zn system 1:1 molar ratio by changing the pH and in Fig. 7S the NMR plots for ^{13}C chemical shift δΔ variations for the SC:Zn system 1:1 molar ratio by changing the pH are reported, respectively.

3.7. X-ray structures of tren complexes

In the following, we report on the structures of the complexes formed by tren with zinc, copper and iron. Fig. 19 reports the X-ray structures of the complexes formed by tren with zinc [35], copper [36] and iron [37] respectively. The length of the bonds between the metal ions and the apical nitrogen atom, and the three terminal nitrogen atoms, are reported in Table 7.

3.8. DFT calculations

The Metal-SC complexes with Zn^{2+} and Al^{3+} ions were initially studied for computational convenience since they are systems with singlet multiplicity. Furthermore, they are good for comparisons, as they have the highest and the lowest stability of the 1:1 complex experimentally found with SC. In Fig. 20 the minimum energy structures of the ZnS complex are displayed: the structures a) and b) have been

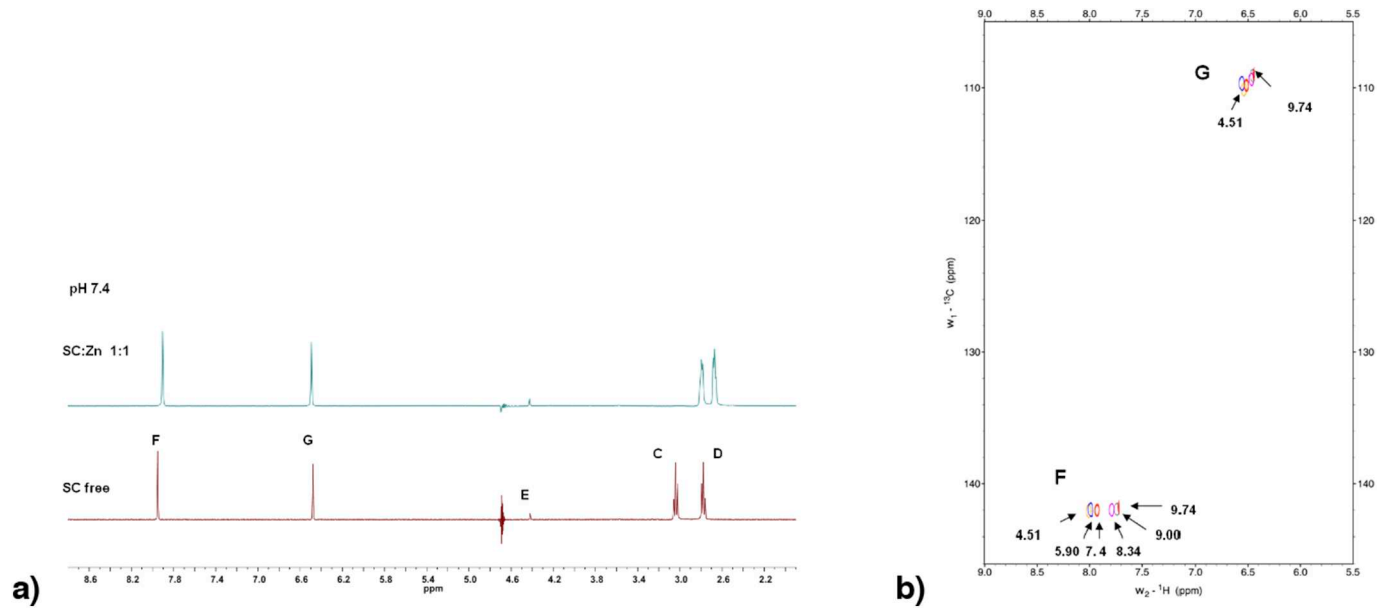

Fig. 18. a) Spectrum of free ligand SC (lower spectrum) and in presence of an equimolar amount of Zn^{2+}, at pH 7.4; b) spectra ^{1}H-^{13}C-HSQC of the system SC:Zn (1:1) at different pH values.

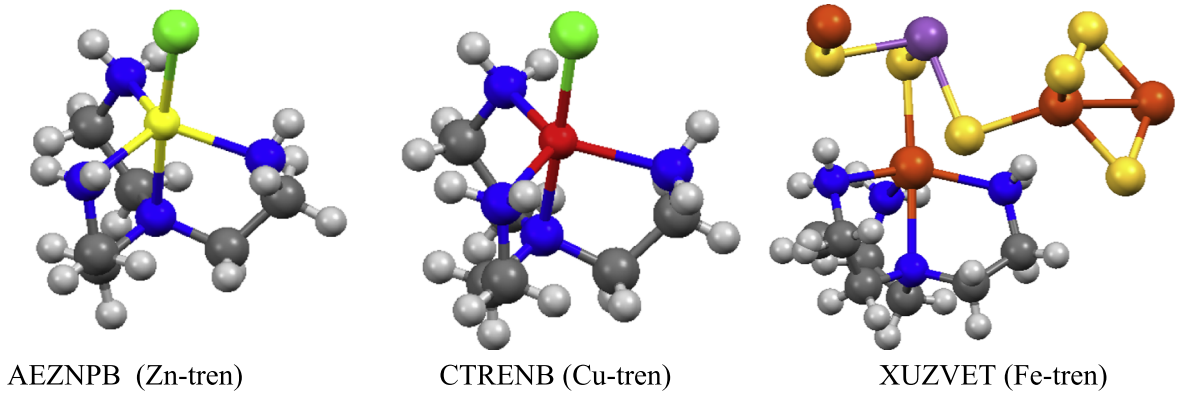

Fig. 19. X-Ray structures of the tren complexes with zinc, copper and iron. Coordinates obtained from the Cambridge Structural Database, images created with Mercury3.5.

Table 7
The length of the bonds between the metal ions (zinc, copper and iron) and the nitrogen atoms: the apical nitrogen atom, and the three terminal nitrogen atoms.

	Zinc	Copper	Iron
Apical N atom	2.325	2.080	2.302
NH_2 (1)	2.062	2.107	2.149
NH_2 (2)	2.067	2.066	2.135
NH_2 (3)	2.064	2.099	2.149

optimized without additional water molecules to saturate the first coordination sphere of the metal ion while three additional water were introduced in c). It results that the a) structure has an energy of ~55 kcal mol^{-1} higher than b) therefore the a) coordination mode can be discarded for this species. This result is in agreement with the observed changes of the aromatic F and G protons at pH > 8 (Fig. 17), supporting the hypothesis that at lower pH coordination occurs preferentially at the N atoms of the linker, while at higher pH values the KA units are involved. Geometry searches always led to complexes where the KA moieties are not completely coordinated to the metal, but they can be either mono or bidentate. In the c) complex, the addition of the water molecules leads to the opening of the bidentate KA moiety.

In the case of Al^{3+}, the d) structure is less stable than e) by ~135 kcal mol^{-1} thus it is discarded also in this case and compatible with the observed preferential interaction with the oxygen atoms occurring at low pH yet. It should be noted that in e) the ligand can be bidentate with two KA units.

When also two water molecules are considered, one KA moiety opens to become monodentate. In summary, it can be concluded that: i)

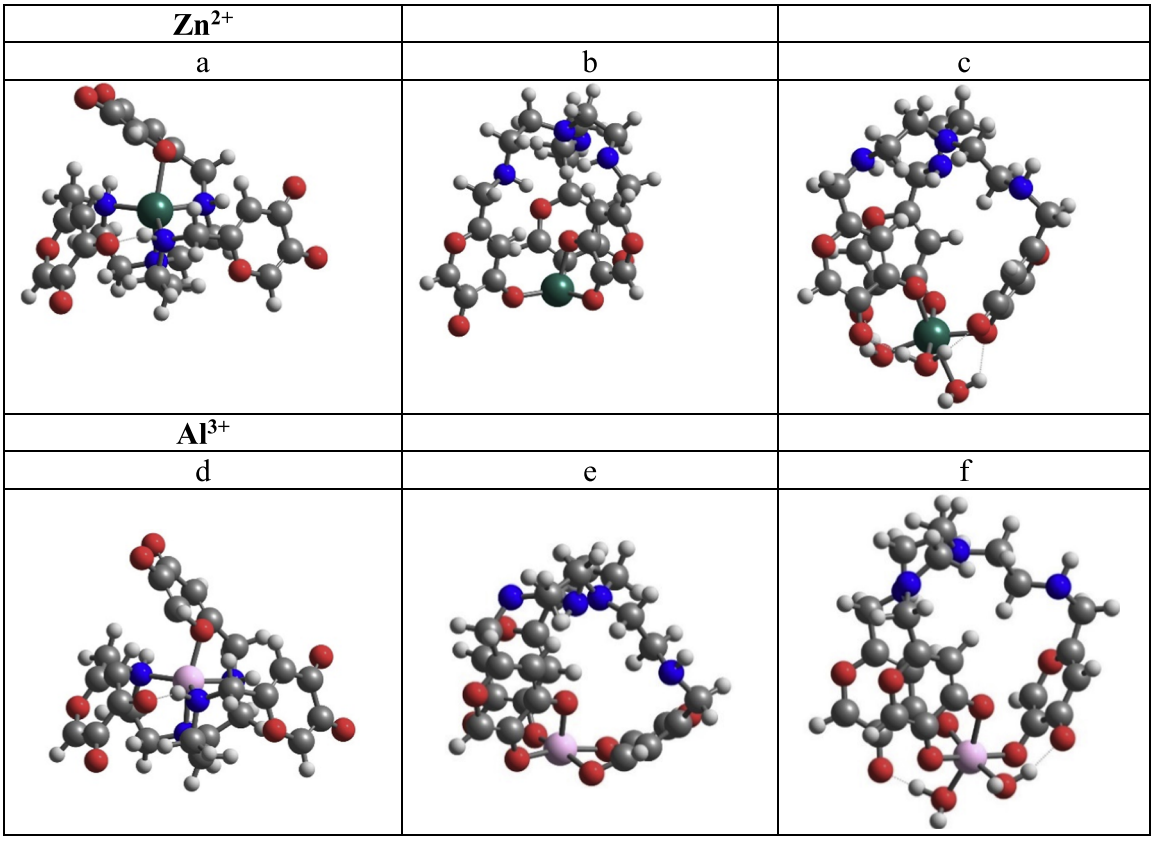

Fig. 20. Possible coordination modes of Zn^{2+} and Al^{3+} ions in the 1:1 complexes obtained in gas phase.

Table 8
Biodistribution of ^{67}Ga in the most relevant organs, expressed as percentage of I. A./g, after administration of ^{67}Ga-citrate with simultaneous intraperitoneal injection of SC ligand, at 1, and 24 h post-injection in female CD-1 mice (n = 3).

	^{67}Ga-SC	
	1 h	24 h
Blood	2.0 ± 0.6	0.8 ± 0.2
Liver	3.1 ± 0.6	1.1 ± 0.7
Intestine	2.1 ± 0.5	0.5 ± 0.4
Spleen	1.5 ± 0.4	0.5 ± 0.3
Heart	0.8 ± 0.2	0.7 ± 0.6
Lung	1.4 ± 0.4	1.2 ± 0.1
Kidney	3.6 ± 0.5	2.3 ± 0.5
Muscle	0.5 ± 0.1	0.21 ± 0.05
Bone	4.9 ± 1.3	0.6 ± 0.5
Stomach	1.2 ± 0.4	0.3 ± 0.2
Excretion (% I.A.)	49.9 ± 5.8	79.3 ± 5.5

the ligand is not flexible enough to encapsulate efficiently the metal ions ii) only the KA groups are involved in the complexation reaction, iii) Al^{3+} ion interacts more efficiently with the ligand due to the formation of more bonds with the KA units.

The same calculation carried out for Fe^{3+} ion provided a structure similar to that of Al^{3+} ion (Fig. 8S). By comparing the theoretical spectra of the FeSC complex (Fig. 9S) with that of the $Fe(KA)_3$ species it emerges that they are different confirming that the coordination mode should be different in the two cases.

3.9. Biological assays

Biodistribution studies were carried out in CD-1 mice to assess the efficacy of the ligand as chelating agent for the mobilization of gallium in ^{67}Ga-citrate injected mice. Since the biodistribution profile of the radiotracer ^{67}Ga-citrate in mice is well-known, we evaluated the effect of the ligand on the biokinetics and elimination of the radiometal by intraperitoneal administration of 0.5 μmole of the SC solution immediately after intravenous administration of the radiotracer. Tissue distribution of ^{67}Ga in major organs at 1 h and 24 h expressed as % I.A./g is presented in Table 8 and Fig. 21.

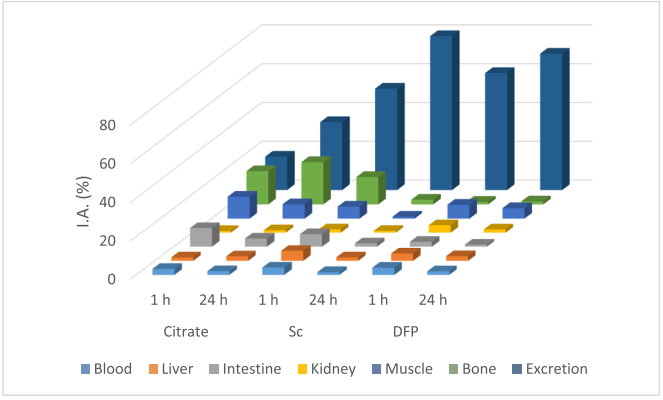

Fig. 21. Biodistribution data in the most relevant organs, expressed as % I. A. for ^{67}Ga-citrate and ^{67}Ga-citrate with co-administration of DFP or SC at 1 and 24 h after administration in female CD-1 mice (n = 3).

These results indicate that the radiometal is rapidly cleared from the bloodstream through both the hepatobiliary and the urinary excretory pathways. Clearance from the major organs is rapid and most of the radioactivity was eliminated at 24 h after injection, except in the organs related with the excretory tracts, liver and kidneys. The overall rate of radioactivity excretion was moderate, 49.9 ± 5.8 and 79.3 ± 5.5% I.A, at 1 h and 24 h, respectively. Altogether, these results in mice demonstrated that the ligand has *in vivo* chelating ability promoting the elimination of the radiometal from the animal body.

To further evaluate the effect of our ligand on the ^{67}Ga distribution and excretion and its usefulness to complex *in vivo* and eliminate unwanted trivalent metal ions, we have compared our results with those found with the drug deferiprone (DFP) in the same animal model at 1 h and 24 h (Fig. 21). Biodistribution profile of the radiotracer ^{67}Ga-citrate without simultaneous administration of any ligand is also included in the graphic for comparative purposes.

Data analysis at 1 h and 24 h after administration evidenced that the co-administration of the ligand has enhanced the clearance of the radiometal ^{67}Ga from most organs, except in the kidneys and the overall excretion rate of radioactivity from whole animal body more efficiently than the drug ($\rho < 0.01$) at 24 h.

In conclusion, this ligand can efficiently chelate the radiometal in our animal model suggesting that it can be a promising candidate as chelating agent of other trivalent metals.

3.10. Pharmacokinetic properties

To evaluate the drug-likeness of the ligand SC, in comparison with the drug DFP (Fig. 1), some descriptors of their pharmacokinetic profiles were calculated using QikProp program, v. 2.5 [38], and are summarized in Table 9. Analysis of the data in this table shows that, although only DFP present no violations to the criteria of the Lipinski's rule [11], SC presents three minor violations of that rule, namely molecular weights (~518.5), lipophilicity (clog $P_{O/W} = -2.57$), slightly exceed the number of H-bond acceptors (16) or H-bond donors (6). Furthermore SC present good capacity for membrane permeation as indicated by log BB values (> -3.113), good binding interaction with Human serum albumin (log $K = -1.064$), and moderate % Human oral absorption (32) by the gastrointestinal (GI) track [38].

Although some molecular descriptors as the molecular weight of the new ligand (572 Da) may put some limits to its possible use as an oral chelating agent, namely based on Lipinski rule [11], but we can consider other type of administration or the use of carriers (ex: nanoparticles, liposomes) to facilitate the drug crossing of the blood-brain barrier. On the other hand, it can find a number of applications in environmental remediation [2–4] and in agriculture for supplying essential elements to plants in an absorbable form, or making easily available those elements already present in the soil [5,6].

4. Concluding remarks

A new tripodal KA derivative (tris-3-hydroxy-4-pyrone) is presented herein and studied for its capacity to chelate iron and aluminium as well as the biometal ions copper and zinc. As compared with other reported tris-chelating ligands [25,32], it is remarkable the easy, cheap and high yield synthesis of this ligand as well as its hydrolytic stability due to absence of amide bonds. The measured protonation constants of

Table 9
Pharmacokinetic properties as predicted *in silico* by software QikProp v.2.5 [38].

Comp.	MW	Donors H bonds	Acceptors H bonds	clog*P* O/W	log*K* HSA serum binding	log BB	% Human oral absorpt. GI
DFP	139	1	3.25	0.601	−0.554	−0.296	78
SC	518.5	6	16.2	−2.571	−1.064	−3.113-	32

KA units do not move away significantly from that of KA, giving evidence of the absence of stabilizing hydrogen bonding. Analogously, the protonation constants related to the nitrogen atoms in the linker strictly resemble those of the tren parent molecule.

Concerning the iron and aluminium complexation, potentiometric, spectrophotometric and NMR results are clearly consistent with the formation of 1:1 metal complexes with differently protonated complexes, although DFT calculations indicate that the simultaneous coordination of the trivalent metal ions by three KA units on the same molecule appears difficult. The formation of differently protonated polynuclear complexes has to be assumed, even if no direct experimental evidence with ESI-MS was reached for the characteristic of SC ligand that prevented such measurements.

Biodistribution studies were carried out to assess the mobilization of gallium in ^{67}Ga-citrate injected mice. These studies demonstrated that this ligand efficiently chelates the radiometal in our animal model, which suggests that it can be a promising candidate as chelating agent of other trivalent metals. The calculated pM trend is $Fe^{3+} > Al^{3+} > Cu^{2+} > Zn^{2+}$ revealed for this ligand a higher chelating efficacy toward Fe^{3+} and Al^{3+} than the divalent biological metal cations, thus indicating that the sequestration of iron does not lead to the depletion of these bio relevant bi-charged metal ions. Furthermore, the high stability of Zn^{2+} complexes can open new perspectives for environmental and clinical applications of SC ligand.

Acknowledgements

VMN and MAZ acknowledge the financial support by MIUR-PRIN 2015 - 2015MP34H3. VMN thanks Fondazione Banco di Sardegna and Regione Autonoma della Sardegna for the financial support “Progetti Biennali di Ateneo Annualità 2016”. The authors from (IST) University of Lisbon acknowledge the Portuguese “Fundação para a Ciência e a Tecnologia (FCT)” for the projects UID/QUI/00100/2013 and PEst-C/SAU/LA0001/2011-2013.

Supplementary data

Supplementary data to this article can be found online at https://doi.org/10.1016/j.jinorgbio.2019.01.012.

References

[1] V.M. Nurchi, G. Crisponi, J.I. Lachowicz, S. Medici, M. Peana, M.A. Zoroddu, J. Trace Elem. Med. Biol. 38 (2016) 10–18.
[2] D. Leštan, C.L. Luo, X.D. Li, Environ. Pollut. 153 (1) (2008) 3–13.
[3] G. Chauhan, K. Pant, K. Nigam, Environ. Sci.: Processes Impacts 17 (1) (2015) 12–40.
[4] A. Serrano, F. Pinto-Ibieta, A. Braga, D. Jeison, R. Borja, F. Fermoso, Environ. Technol. 38 (24) (2017) 3137–3144.
[5] G. Dal Corso, A. Manara, S. Piasentin, A. Furini, Metallomics 6 (10) (2014) 1770–1788.
[6] E. Bloem, S. Haneklaus, R. Haensch, E. Schnug, Sci. Total Environ. 577 (2017) 166–173.
[7] V.M. Nurchi, J.I. Lachowicz, G. Crisponi, Murgia Sergio, M. Arca, A. Pintus, P. Gans, J. Niclos-Gutierrez, A. Domınguez-Martın, A. Castineiras, M. Remelli, Z. Szewczuk, T. Lis, Dalton Trans. 40 (2011) 5984–5998.
[8] L. Toso, G. Crisponi, V.M. Nurchi, M. Crespo-Alonso, J.I. Lachowicz, M.A. Santos, S.M. Marques, J. Niclós-Gutiérrez, J.M. González-Pérez, A. Domínguez-Martín, D. Choquesillo-Lazarte, Z. Szewczuk, J. Inorg. Biochem. 127 (2013) 220–231.
[9] V.M. Nurchi, G. Crisponi, J.I. Lachowicz, S. Murgia, T. Pivetta, M. Remelli, A. Rescigno, J. Niclós-Gutíerrez, J.M. González-Pérez, A. Domínguez-Martín, J. Inorg. Biochem. 104 (2010) 560–569.
[10] V.M. Nurchi, G. Crisponi, J.I. Lachowicz, M.G. Jaraquemada-Pelaez, C. Bretti, M. Peana, S. Medici, M.A. Zoroddu, J. Inorg. Biochem. 189 (2018) 103–114.
[11] C.A. Lipinski, F. Lombardo, B.W. Dominy, P.J. Feeney, Adv. Drug Deliv. Rev. 23 (1997) 3–25.
[12] W.R. Harris, K.N. Raymond, F.L. Weitl, J. Am. Chem. Soc. 103 (1981) 2667–2675.
[13] A. Albert, E.P. Serjeant, Ionization Constants of Acids and Bases: A Laboratory Manual, Methuen, (1962).
[14] R. Silvagni, 2001 University of Sassari, PhD Thesis, pp. 57–58.
[15] G. Gran, Analyst 77 (1952) 661–671.
[16] P. Gans, A. Sabatini, A. Vacca, Talanta 43 (1996) 1739–1753 http://www.hyperquad.co.uk/HQ2013.htm.
[17] C. Frassineti, S. Ghelli, P. Gans, A. Sabatini, M.S. Moruzzi, A. Vacca, Anal. Biochem. 231 (1995) 374–382 http://www.hyperquad.co.uk/HypSpec2014.htm.
[18] M.A. Zoroddu, M. Peana, S. Medici, Dalton Trans. (2007) 379–384.
[19] J.I. Lachowicz, V.M. Nurchi, G. Crisponi, M.G. Jaraquemada-Pelaez, M. Arca, A. Pintus, M.A. Santos, C. Quintanova, L. Gano, Z. Szewczuk, M.A. Zoroddu, M. Peana, A. Dominguez-Martin, D. Choquesillo-Lazarte, Dalton Trans. 45 (2016) 6517–6528.
[20] M. Peana, S. Medici, V.M. Nurchi, J.I. Lachowicz, G. Crisponi, M. Crespo-Alonso, M.A. Santos, M.A. Zoroddu, J. Inorg. Biochem. 148 (2015) 69–77.
[21] A.D. Becke, J. Chem. Phys. 98 (1993) 1372–1377.
[22] C.T. Lee, W.T. Yang, R.G. Parr, Phys. Rev. B 37 (1988) 785–789.
[23] V.M. Nurchi, G. Crisponi, J.I. Lachowicz, M.A. Zoroddu, M. Peana, S. Medici, D. Veclani, M. Tolazzi, A. Melchior, Eur. J. Pharm. Sci. 93 (2016) 380–391.
[24] F. Piccinelli, M. Bettinelli, A. Melchior, C. Grazioli, M. Tolazzi, Dalton Trans. 44 (2015) 182–192.
[25] A.C. Mendonça, A.F. Martins, A. Melchior, S.M. Marques, S. Chaves, S. Villette, S. Petoud, P.L. Zanonato, M. Tolazzi, C.S. Bonnet, É. Tóth, P. Di Bernardo, C.F.G.C. Geraldes, M.A. Santos, Dalton Trans. 42 (2013) 6046–6057.
[26] S. Del Piero, P. Di Bernardo, R. Fedele, A. Melchior, P. Polese, M. Tolazzi, Eur. J. Inorg. Chem. 18 (2006) 3738–3745.
[27] A. Melchior, C. Gaillard, S. Gràcia Lanas, M. Tolazzi, I. Billard, S. Georg, L. Sarrasin, M. Boltoeva, Inorg. Chem. 55 (7) (2016) 3498–3507.
[28] P.J. Hay, W.R. Wadt, J. Chem. Phys. 82 (1985) 270–283.
[29] M.J. Frisch, G.W. Trucks, H.B. Schlegel, G.E. Scuseria, M.A. Robb, J.R. Cheeseman, G. Scalmani, V. Barone, G.A. Petersson, H. Nakatsuji, X. Li, M. Caricato, A.V. Marenich, J. Bloino, B.G. Janesko, R. Gomperts, B. Mennucci, H.P. Hratchian, J.V. Ortiz, A.F. Izmaylov, J.L. Sonnenberg, D. Williams-Young, F. Ding, F. Lipparini, F. Egidi, J. Goings, B. Peng, A. Petrone, T. Henderson, D. Ranasinghe, V.G. Zakrzewski, J. Gao, N. Rega, G. Zheng, W. Liang, M. Hada, M. Ehara, K. Toyota, R. Fukuda, J. Hasegawa, M. Ishida, T. Nakajima, Y. Honda, O. Kitao, H. Nakai, T. Vreven, K. Throssell, J.A. Montgomery, J.E. Peralta, F. Ogliaro, M.J. Bearpark, J.J. Heyd, E.N. Brothers, K.N. Kudin, V.N. Staroverov, T.A. Keith, R. Kobayashi, J. Normand, K. Raghavachari, A.P. Rendell, J.C. Burant, S.S. Iyengar, J. Tomasi, M. Cossi, J.M. Millam, M. Klene, C. Adamo, R. Cammi, J.W. Ochterski, R.L. Martin, K. Morokuma, O. Farkas, J.B. Foresman, D.J. Fox, Gaussian 16 Rev.A03 Wallingford, CT, (2016).
[30] F. Weigend, R. Ahlrichs, Phys. Chem. Chem. Phys. 7 (2005) 3297–3305.
[31] F. Neese, The ORCA program system, Wiley Interdiscip. Rev.: Comput. Mol. Sci. 2 (1) (2012) 73–78.
[32] R. Cappai, K. Chand, J.I. Lachowicz, S. Chaves, L. Gano, G. Crisponi, V.M. Nurchi, M. Peana, M.A. Zoroddu, M.A. Santos, New J. Chem. 42 (2018) 8050–8061.
[33] V.M. Nurchi, G. Crisponi, G. Sanna, M.I. Pérez-Toro, J. Niclos-Gutierrez, M.J. Gonzalez-Perez, A. Dominguez-Martin, Complex Formation Equilibria between polyamine ligands and copper(II) and zinc(II), J. Inorg. Biochem. (2019) (submitted for publication).
[34] http://www.hyperquad.co.uk/hyss.htm.
[35] A. Zalkin, R.J. Sime, R.P. Dodge, David H. Templeton, Inorg. Chem. 10 (3) (1971) 537–541.
[36] E.J. Laskowski, D.M. Duggan, D.N. Hendrickson, Inorg. Chem. 14 (10) (1975) 2449–2459.
[37] R. Kiebach, W. Bensch, R.D. Hoffmann, R. Pöttgen, Z. Anorg. Allg. Chem. 629 (2003) 532–538.
[38] QikProp, Version 2.5, Schrödinger, LLC, New York, NY, 2005.